Performance of the LHCb RICH photo-detectors and readout in a system test using charged particles from a 25 ns-structured beam

M. Adinolfi [a], E. Albrecht [b], C. D'Ambrosio [b], T. Gys [b], J. Morant [b], D. Piedigrossi [b], M. Patel [b], K. Wyllie [b], M. Ameri [c], F. Fontanelli [c], G. Mini [c], M. Sannino [c], C. Arnaboldi [d], T.F. Bellunato [d], E. Fanchini [d], D.L. Perego [d], G. Pessina [d], C. Barham [e], C. Buszello [e], J. Dickens [e], V. Gibson [e], C. Jones [e], U. Kerzel [e,*], G. Rogers [e], H. Skottowe [e], S. Wotton [e], T. Blake [f], C. Eames [f], R. Plackett [f], S. Brisbane [g], N. Harnew [g], J. Libby [g], A. Powell [g], P. Sullivan [g], S. Topp-Jorgensen [g], S. Easo [h], A. Papanestis [h], Z. Zhang [h], S. Eisenhardt [i], F. Muheim [i], N. Styles [i]

[a] H.H. Wills Physics Laboratory, University of Bristol, Tyndall Avenue, Bristol BS8 1TL, UK
[b] CERN, EP Division, 1211 Geneva 23, Switzerland
[c] Università di Genova and Sezione INFN, Genova, Italy
[d] Università di Milano-Bicocca and Sezione INFN, Milano, Italy
[e] Cavendish Laboratory, University of Cambridge, JJ Thomson Avenue, Cambridge CB3 0HE, UK
[f] Physics Department, Imperial College London, London SW7 2AZ, UK
[g] University of Oxford, Denys Wilkinson Building, Keble Road, Oxford OX1 3RH, UK
[h] Rutherford Appleton Laboratory, Chilton, Didcot, Oxon, OX11 0QX, UK
[i] School of Physics, University of Edinburgh, Mayfield Road, Edinburgh EH9 3 JZ, UK

ARTICLE INFO

ABSTRACT

The LHCb experiment at the CERN Large Hadron Collider (LHC) utilises two Ring Imaging CHerenkov (RICH) detectors for particle identification. To verify that the RICH assembly will perform as expected prior to installation, an array of 48 production Hybrid Photon Detectors and their readout have been tested under realistic running conditions in a 25 ns-structured charged particle beam provided by the SPS facility at CERN. This system test is an important milestone in the overall commissioning of the LHCb detector and demonstrates that all aspects meet the stringent physics requirements of the LHCb experiment.

© 2009 Elsevier B.V. All rights reserved.

1. Introduction

The LHCb experiment [1] at the CERN Large Hadron Collider (LHC) is optimised for high precision measurements of the charm and beauty quark sectors. Its particle identification capabilities are unique among the four LHC experiments. Central to the LHCb particle identification strategy are two Ring Imaging CHerenkov (RICH) detectors [2]. The upstream detector, RICH 1, uses aerogel and C_4F_{10} Cherenkov radiators, whilst the downstream detector, RICH 2, is filled with CF_4 gas. The RICH system uses custom-built pixel Hybrid Photon Detectors (HPDs) [3], developed in close collaboration with industry,[1] to measure Cherenkov photons over the wavelength range 200–600 nm. Previous beam-tests [4] have successfully demonstrated the design of individual components and verified that they are able to fulfil the stringent requirements posed by the challenging LHCb physics programme. To test the overall performance of the final components and exercise the complete RICH operation and data-acquisition, a beam-test has been performed in September 2006 at the SPS facility at CERN. The structure of the particle beam provided by the accelerator has been configured to match the 25 ns beam-structure of the LHC.

* Corresponding author. Cavendish Laboratory (HEP group), JJ Thomson Avenue, Cambridge CB3 0HE, UK.
E-mail address: Ulrich.Kerzel@cern.ch (U. Kerzel).

[1] Photonis-DEP, BV, NL-9300 AB Roden, Netherlands as main industrial partner.

The data have been recorded using prototype versions of the LHCb online software and the subsequent analysis has been performed using the LHCb offline reconstruction and analysis framework. Simulated events have been obtained from the LHCb simulation software which has been modified to reflect the experimental setup of the beam-tests.

The experimental setup used during the beam-tests is illustrated in Fig. 1. A beam consisting of mainly 80 GeV/c negatively charged pions was extracted from the SPS and directed through the light-tight radiator vessel. Cherenkov photons generated by the particles traversing the radiator were reflected to the photo-detectors using an adjustable parabolic mirror (with focal length $f = 1.016$ m). The photo-detectors are fixed at a distance of 1.047 m from the mirror centre. Both the radiator vessel and the mirror have been specifically designed for the beam-tests and have already been used in previous studies [4].

An HPD consists of a pixelated silicon detector anode assembly which is encapsulated in a vacuum envelope as illustrated in Fig. 2. The HPDs are produced in a high vacuum of typically 1.3×10^{-7} Pa. The silicon sensor chip is divided into 256×32 pixels, each $62.5\,\mu\text{m} \times 500\,\mu\text{m}$ in size. Groups of eight pixels are OR-ed together creating 1024 logical pixels of $500\,\mu\text{m} \times 500\,\mu\text{m}$. The photo-electrons detected by the pixels on the silicon sensor are read out as a binary signal, i.e. the pixel is considered to have been hit if the detected signal exceeds a given threshold. The HPD vacuum tube has a 7 mm thick quartz entrance window coated with an S20 multi-alkali photo-cathode on the inside. The active diameter of the spherical entrance window is 75 mm.
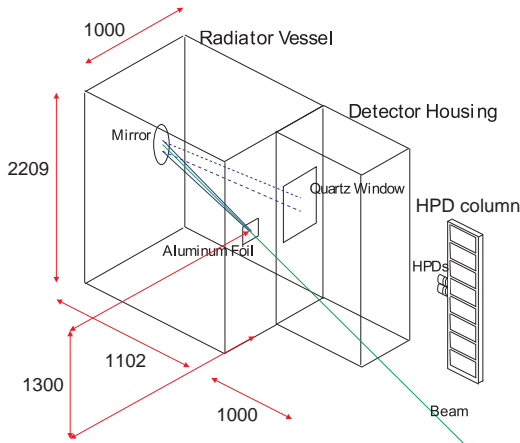

Fig. 1. Schematic overview of the setup of the RICH detector used in the beam-test. Dimensions are in mm.
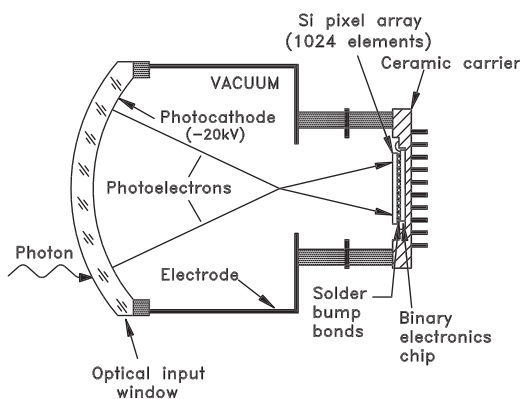

Fig. 2. Schematic overview of a Hybrid Photon Detector (HPD).

Photo-electrons emitted from the photo-cathode are accelerated towards the silicon pixel detector by a cross-focusing electrostatic field generated by electrodes at 20 kV. The resulting image on the silicon detector is de-magnified by a factor of ≈ 5 and the size of the image on the silicon sensor directly influences the magnitude of the measured Cherenkov angle. A precise determination of the de-magnification parameters is, therefore, a necessary prerequisite in the calibration of the RICH detector. The parameters have been determined in the laboratory by mounting a blue LED on an x–y translation table system with micro-metric precision. The translation tables were moved over the full active diameter of an HPD and the resulting de-magnification properties are parameterised as

$$r_P = \alpha \cdot r_C + \beta \cdot r_C^2$$

where the radial cathode and pixel coordinates r_C and r_P are expressed in mm as illustrated in Fig. 3. The linear term, $\alpha = 1.958 \times 10^{-1} \pm 7.863 \times 10^{-3}$, describes the linear de-magnification, whereas the small quadratic term, $\beta = ((-5.206 \pm 2.800) \times 10^{-4})\,\text{mm}^{-1}$ is related to effects such as edge distortions. The error bars correspond to the arrival coordinates for two photo-electrons with a 1 eV initial kinetic energy and emitted at $\pm 45°$ from the normal to the photo-cathode surface. Fig. 3 shows that the measured de-magnification properties are in good agreement with the description obtained using the POISCR simulation package [5–7]. A possible de-centering of the silicon anode relative to the electro-static axis is taken into account in the alignment step described in detail in Section 2. Due to the compact setup used in the beam-tests, the reconstructed Cherenkov angle is sensitive to the numerical values of the measured de-magnification parameters within the quoted uncertainties, especially for the case of N_2 where the Cherenkov ring is fully contained within a single HPD.

A pair of HPDs is connected to the "Level-0" front-end electronics board [8], mounted on-detector. The HPDs and Level-0 boards are then mounted onto columns which also include low- and high-voltage boards [9,10] to power the HPDs. Each HPD is enclosed by a mu-metal shield to later protect the photo-detector from the magnetic field of the LHCb spectrometer. In RICH 1, 14 columns in a close-packed arrangement each hold 14 HPDs, together with the on-detector electronics and voltage supplies. In RICH 2, 18 columns each hold 16 HPDs. Fig. 4 shows a photograph of a fully assembled column.
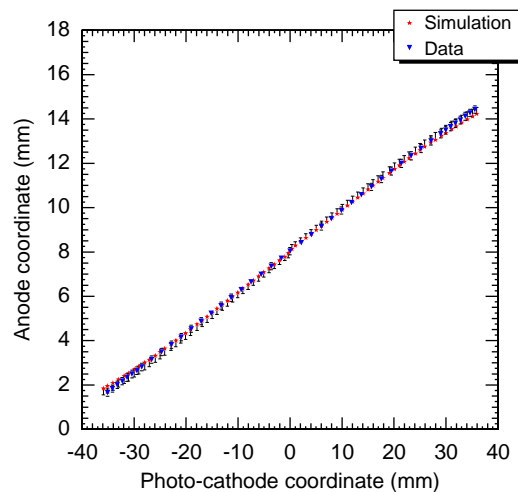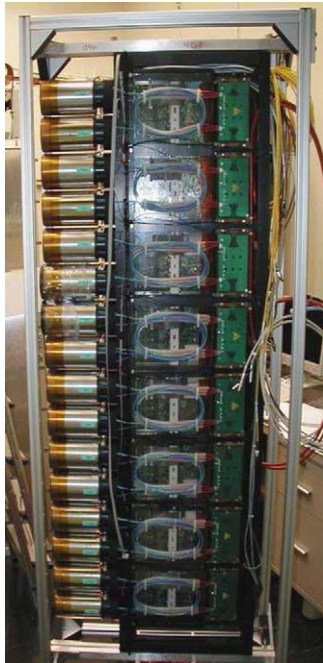

Fig. 3. De-magnification of the HPDs which can be described by a second degree polynomial.

The synchronisation of the front-end electronics and the local distribution of the clocks and trigger are performed on the Level-0 board using the Timing, Trigger and Control Receiver ASIC (TTCrx) [11]. Following a Level-0 trigger accept, the data from a pair of HPDs are multiplexed out at a 40 MHz rate as two 32-bit streams onto optical links to the off-detector (Level-1) electronics [1]. The multiplex grouping of 32 is chosen to match the maximum average LHCb Level-0 trigger rate of 1 MHz.

In the beam-tests, three columns were equipped with a total of 48 HPDs and 24 Level-0 boards from the final LHCb production. The off-detector (Level-1) electronics were taken from production pre-series. Using the 25 ns beam-structure of the SPS, the tests, therefore, provide a unique opportunity to exercise the RICH operations and data-acquisition with final or nearly final components in a timing and control environment identical to the operating conditions of the LHCb experiment.

Two bare silicon pixel anodes from the HPD production were equipped with readout electronics and were placed upstream and downstream of the RICH gas enclosure along the beam line. Using this setup, the position of the beam particle traversing the detector was obtained at two points, thereby allowing the particle trajectory to be represented by a straight line between the silicon pixel sensors. The pixel chips were connected to the same Level-0 data-acquisition electronics used for the HPDs and hence were read out in an identical manner.
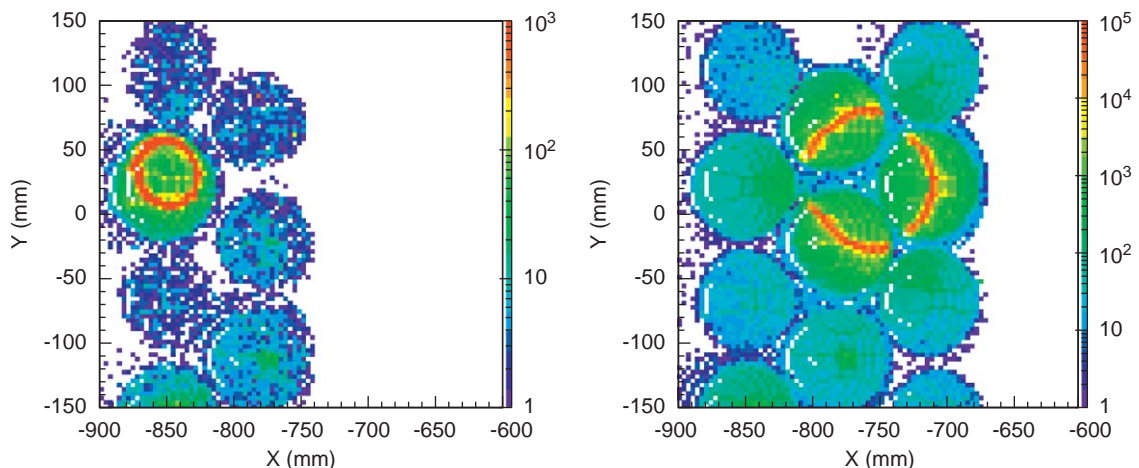
The gas radiator volume was either filled with N_2 or C_4F_{10} during the beam-tests. In the case of N_2 ($n \approx 1.0003$), the average diameter of the Cherenkov ring at the photo-detector plane was 43 mm and hence its image could be contained on a single HPD as illustrated by Fig. 5 (left). The refractive index of C_4F_{10} is ≈ 1.0014, which corresponds to a Cherenkov angle of 50 mrad. Due to the high beam energy, the emitted Cherenkov radiation is saturated and the different particle species can no longer be separated. The resulting Cherenkov ring spanned up to four HPDs as illustrated in Fig. 5 (right). The use of C_4F_{10} has a twofold advantage. Firstly, the same gas is used in RICH 1, so that results from the beam-test can be easily translated to LHCb performance. Secondly, since the resulting Cherenkov ring is shared between up to four HPDs, the timing, alignment and performance can be studied on multiple photo-detectors simultaneously.

The expected Cherenkov angle is determined from the refractive index of the medium which is parameterised using Sellmeier coefficients [13]. In the case of C_4F_{10}, the numerical values of the coefficients are determined by a fit to data measured in the DELPHI experiment [14]. The numerical values in the case of N_2 are taken from [15].

Simulated events for the test-beam study have been obtained using the official LHCb simulation package based on the GEANT4 [16] toolkit. Compared to the default LHCb configuration, only the representation of the detector and the beam have been changed. The analysis of the data recorded at the beam-tests, therefore, provided a significant milestone in the validation of the simulation software.

2. Alignment

During the beam-tests, the position and orientation of the mirror was changed between different periods of data-taking to illuminate different HPDs. From a study of simulated events, it was found possible to determine mirror rotation misalignments accurately from the reconstructed data without relying on the underlying true input values [17]. Any misalignment leads to a sinusoidal variation of the Cherenkov angle, θ_C, as a function of

Fig. 4. A photograph of a fully assembled HPD column, with HPDs, on-detector electronics (Level-0) and high- and low-voltage supplies.

Fig. 5. Cherenkov rings imaged on the photo-detector plane from N_2 (left) and C_4F_{10} (right) radiators.
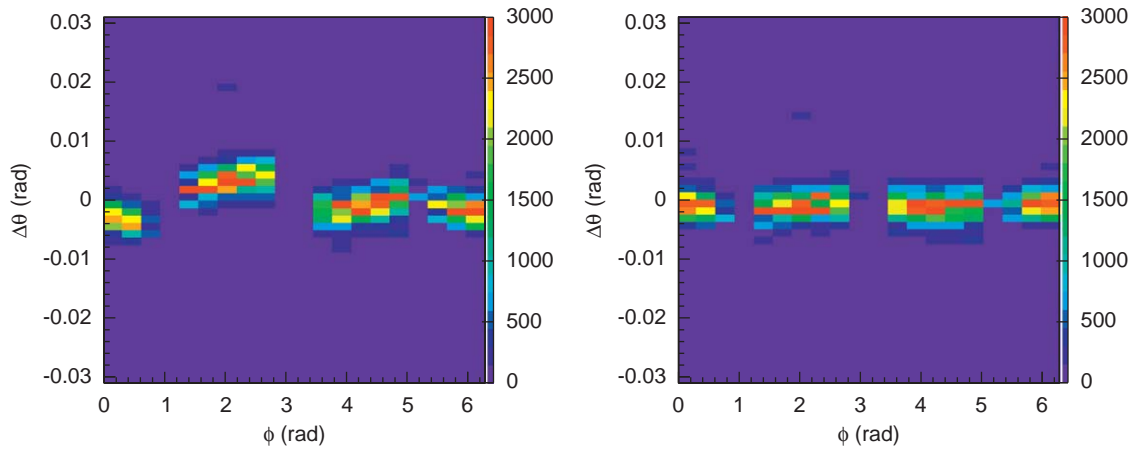
Fig. 6. Difference of the measured Cherenkov angle and expected angle ($\Delta\theta_C$) as a function of the angle around the Cherenkov ring ϕ_C with a C_4F_{10} radiator after preliminary mirror alignment (left) and full alignment (right).

the azimuthal angle, ϕ_C, measured around the ring in the photo-detector plane. The detector geometry is then corrected during the alignment procedure such that the distribution of θ_C as a function of ϕ_C becomes constant. In addition to effects due to mirror misalignments, contributions from the relative positioning of HPDs and the silicon sensors inside the HPDs are taken into account. This is illustrated in Fig. 6 which shows the distribution of the difference of the measured Cherenkov angle and the expected angle, $\Delta\theta_C$, after the mirror has been aligned (left) and the resulting flat distribution after the full alignment procedure (right).

3. Photon yield

3.1. Event selection and fit model

A key quantity in the evaluation of the efficiency of the RICH detector is the average number of photons detected per incident particle (the photon yield). The following effects, each discussed below, need to be considered in the determination of the photon yield:

- ion feedback;
- field settling effects;
- double hits;
- pixel-to-pixel charge-sharing and
- beam composition.

An _ion feedback_ signal occurs when a photo-electron scatters from a residual atom inside the HPD vacuum tube producing an ion which is slowly accelerated back towards the photo-cathode. When an ion hits the photo-cathode the resulting electrons are accelerated towards the pixelated anode and usually distributes charge across many pixels. Due to the cross-focusing setup of the HPD, hits originating from ion feedback tend to be concentrated at the centre of the silicon pixel detector.

Hits due to _field settling effects_ are concentrated around the edge of the photo-cathode image on the pixel chip and occur mainly when the high-voltage is switched on. The stabilising field induces micro-discharges on the surfaces leading to further light emission. As the electrical field inside the HPD settles this effect decreases within a few hours after the high-voltage is applied. Limited beam time and an extensive testing programme meant

that data had to be recorded even though ideal operating conditions had not yet been necessarily met.

To remove the above sources from the determination of the photon yield, hits are only considered if they lie within an annulus region defined by the expected Cherenkov ring. In the case of N_2, rings are fitted to all events on an event-by-event basis and the average ring centre and radius are used to define the valid ring region as ± 3 logical HPD pixels about this average ring position. The same approach is followed in case of C_4F_{10}, using a width of ± 1.5 logical HPD pixels for the annulus. The size of the annulus region is chosen to match the expected variation in ring sizes of the different particle types in both radiator media. At least four hits are required in both analyses within the annulus region and events with more than three hits outside are rejected to limit the contamination by background.

As described in Section 1, only binary values are read out from the silicon pixel chip. If two or more genuine photo-electrons from the same Cherenkov ring strike the same logical pixel, this will be registered in the same way as if only one photo-electron had hit that pixel. Consequently, part of the information will be lost. Using a stand-alone simulation the probability of the _double hit_ effect in N_2 has been estimated to be $(5 \pm 1) \times 10^{-3}$. The effect of triple and multiple hits are negligible. The same factor applies for the case of C_4F_{10} since the number of photons per radian is approximately the same as for N_2. However, the contribution from the double hits is treated as a free parameter in the analysis of the C_4F_{10} photon yield.

The HPD signal produced from the primary photo-electron is usually contained within a single logical pixel of the silicon chip but may give a signal over threshold in two or more adjacent pixels. To measure the probability of this _charge-sharing_ effect, a set of red LEDs is deployed in the experimental setup. The charge-sharing probability was then determined by counting the number of adjacent two-pixel clusters, taking into account a correction due to the probability of two genuine photo-electrons striking adjacent pixels which was estimated from a stand-alone simulation. The systematic uncertainty was evaluated by considering contributions from background sources such as ion feedback and field settling effects, as well as a variation of the nominal size of the photo-cathode image on the silicon sensor by $\pm 5\%$. The results for the HPDs used in the determination of the photon yield are summarised in Table 1.

The SPS beam contains a mixture of particles comprising approximately 80% π^-, 10% electrons, 7% kaons and 3% anti-protons with an estimated uncertainty of 1% [18]. The photo-electron yield is extracted by performing a constrained fit to the

distribution of hit pixels per event

$$N(n) = N_\pi P(n|\mu; s, d) + N_{2\pi} P(n|2\mu; s, d)[+N_{3\pi} P(n|3\mu; s, d)]$$

where $P(n|\mu; s, d)$ is the conditional Poisson probability distribution to observe n photo-electrons given the mean (μ) of the distribution, the contribution from charge-sharing (s) and double-hits (d). The mean (μ), the number of one particle (N_π) and the number of two particle events ($N_{2\pi}$), both assumed to be solely pions, are allowed to vary in the fit. In the case of C_4F_{10}, a three particle contribution $N_{3\pi}$ was also included. The values of the contributions from charge-sharing and, in the case of N_2, double-hits were fixed to the measured values in the fit and varied within their uncertainties to evaluate the size of the systematic uncertainties. For N_2 the beam composition is fixed to the measured values in the fit. Systematic uncertainties are evaluated by varying the relative fraction of particle species in the fit. Given the higher refractive index of C_4F_{10}, the particle species can no longer be disentangled and the fit does not depend on the composition of the beam.
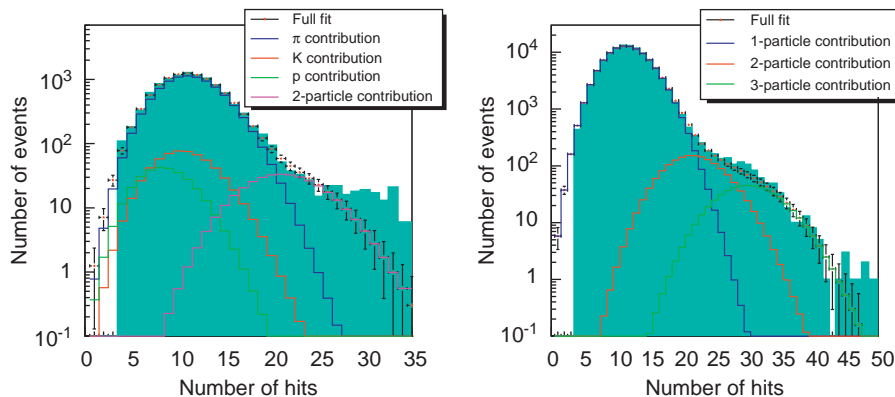
3.2. Photoelectron yield for N_2

An example distribution of the number of hit pixels per event with its corresponding fit for an N_2 run can be seen in Fig. 7 (left). The model accurately reproduces the distribution seen in the data. The residual discrepancy on the right side is attributed to few events with more than two particles passing the selection criteria. Table 2 summarises the measured yields for each of the three photo-detectors for which data are available.

The measured photon yields are compared to the expected yields for each of the HPDs, including the quantum efficiencies measured by the manufacturer, in Table 3. The expected yields contain an additional HPD efficiency factor which mainly results from electron backscattering from the silicon anode which reduces the energy of the cluster. This efficiency has been determined to be $\approx 85\%$ [19]. The largest contributions to the

uncertainty on the expected yield originate from a 5% error on the product of the measured quantum efficiency of the HPDs, the transmission of the quartz window separating the gas radiator from the HPD volume and the reflectivity of the mirror. The quoted uncertainty in Table 3 also includes a small contribution from atmospheric pressure and temperature variations during the beam-test period. The photon yields measured in this beam-test are about 20% higher than reported in the previous tests [4]. Compared to the previous setup, a synchronous beam with a higher energy was used. In addition, the HPDs used in the previous tests were taken from earlier production series whereas the HPDs used in this test have been produced later. Quality control checks have shown that the quantum efficiency with which the incident photon is converted into the primary photo-electron is significantly higher in later produced HPDs due to continuous efforts to improve the production cycle.

3.3. Photo-electron yield for C_4F_{10}

In the case of the C_4F_{10} radiator, the Cherenkov rings are distributed over three or four HPDs. Each photo-detector, therefore, accepts a different portion of the ring and we, therefore, normalise the number of photoelectrons seen in each photo-detector to the azimuthal angle fraction $\Delta\phi$, as measured from the

Table 1
Charge-sharing fractions measured from LED data including statistical and systematic uncertainties.

HPD no.	Charge-sharing fraction (%)
117	$(2.8 \pm 0.0(\text{stat.}) \pm 0.2\ (\text{syst.}))$
222	$(4.1 \pm 0.0(\text{stat.}) \pm 2.0\ (\text{syst.}))$
265	$(1.7 \pm 0.1(\text{stat.}) \pm 1.1\ (\text{syst.}))$
282	$(3.1 \pm 0.1(\text{stat.}) \pm 0.3\ (\text{syst.}))$

Table 2
The fitted hit pixel distribution for three HPDs under study.

HPD	Events	$N_{\pi,K,p}$	$N_{2\pi}$	μ	χ^2/NDF
117	15,290	$14,870 \pm 125^{+27}_{-28}$	$362 \pm 43^{+20}_{-19}$	$12.44 \pm 0.04^{+0.08}_{-0.09}$	23.23/17
264	23,253	$22,756 \pm 155^{+45}_{-60}$	$459 \pm 60^{+68}_{-61}$	$13.08 \pm 0.03^{+0.15}_{-0.12}$	12.47/17
265	20,085	$19,536 \pm 143^{+50}_{-59}$	$491 \pm 50^{+50}_{-49}$	$12.76 \pm 0.03^{+0.16}_{-0.13}$	17.47/17

The first set of uncertainties are the statistical uncertainty on the fitted distribution and the second set are the systematics due to charge sharing, double hits and the beam composition.

Table 3
Measured and expected yields in N_2 at $T = 295\,\text{K}$ and $P = 9.6 \times 10^4\,\text{Pa}$.

HPD	Meas. yield	Exp. yield	Ratio
117	$12.44 \pm 0.04^{+0.08}_{-0.09}$	12.15 ± 0.61	1.02 ± 0.05
264	$13.08 \pm 0.03^{+0.15}_{-0.12}$	13.98 ± 0.70	0.94 ± 0.05
265	$12.76 \pm 0.03^{+0.16}_{-0.13}$	12.72 ± 0.64	1.01 ± 0.05

Fig. 7. The observed number of Cherenkov photons per event (points) and fit (line) measured using N_2 (left) and a mixture of 90.2% C_4F_{10} and 9.8% N_2 (right) as radiators. The figures have been obtained from the fit to a single data run.

centre of the ring, covered by the active part of each photo-cathode.

Due to an imperfect gas circulation system and limited time, data taken with C_4F_{10} have an additional complication of an *a priori* unknown concentration of C_4F_{10} in the gas radiator volume for each run. Fig. 7 (right) illustrates the result of the fit to the photon yield for one run with 90.2% C_4F_{10} and 9.8% N_2. Table 4 summarises the results obtained for two runs of slightly differing C_4F_{10} fractions. The quoted C_4F_{10} molar fraction is extrapolated from the measured mean Cherenkov angle $\langle \theta_C \rangle$.

The systematic uncertainty on the photoelectron yield in C_4F_{10} has been evaluated considering various possible sources. Doubling the width of the annulus from three to six pixels, which is equivalent to doubling the fraction of the HPD area where the hits are counted as signal hits, results in $\sim$3% higher single particle Poisson mean. This indicates that most signal hits are already included in the default selection and hits from background sources contribute at most at the 3% level. The measurement of the fraction of azimuthal angle along the Cherenkov ring covered by the HPD has an uncertainty of about 5%. Relaxing or tightening the fit range and leaving the charge-sharing fraction as a free parameter rather than fixing it to the measured value contributes only 1% to the systematic uncertainty. Overall, the systematic uncertainty in the photon yield per radian for C_4F_{10} is estimated at 5%.

4. Cherenkov angle resolution

The resolution of the reconstructed Cherenkov angle is one of the key parameters in the evaluation of the performance of the

Table 4
Measured and expected yields in C_4F_{10} per unit $\Delta\phi$ for two different runs.

|	HPD	Meas. yield (rad^{-1})	Exp. yield (rad^{-1})	Ratio
90.2% C_4F_{10}	222	8.9 ± 0.5	9.3 ± 0.5	1.0 ± 0.1
$T = 296.45\,K$	265	8.6 ± 0.5	8.9 ± 0.5	1.0 ± 0.1
$P = 9.59 \times 10^4\,Pa$	283	8.7 ± 0.5	9.3 ± 0.5	0.9 ± 0.1
94.7% C_4F_{10}	265	8.9 ± 0.5	9.3 ± 0.5	1.0 ± 0.1
$T = 297.25\,K$	282	9.3 ± 0.6	9.3 ± 0.6	1.0 ± 0.1
$P = 9.60 \times 10^4\,Pa$	283	9.1 ± 0.5	9.6 ± 0.5	1.0 ± 0.1

The yields are normalised to the fraction of the Cherenkov ring covered by each individual HPD in ϕ. The quoted uncertainties contain both statistical and systematic contributions added in quadrature, and is dominated by the systematic contribution.

LHCb RICH detectors. Details of the reconstruction algorithm can be found in Ref. [20].

The Cherenkov angle, θ_C, is reconstructed for each photon hit and is measured with respect to the centre of the ring. The ring centre is measured from the known spatial parameters of the charged particle when imaged onto the photo-detector plane. Fig. 8 shows the distributions of θ_C per track for N_2 and C_4F_{10} radiators. The distributions are obtained by taking the weighted mean of the individual hit measurements associated to a given particle for both data and simulation. Fig. 8 (left) shows the distribution obtained for data taken with the N_2 radiator and Fig. 8 (right) shows the corresponding distribution for C_4F_{10}. The simulated hits for N_2 agree well with the distribution obtained from data and illustrate the high level of precision which we can expect from the RICH detectors of the LHCb experiment. For C_4F_{10}, due to the imperfect knowledge of the exact fraction of C_4F_{10} in the gas admixture, the Sellmeier coefficients (which determine the gas refractive index) were tuned so that the mean Cherenkov angle in the simulated events agreed with the mean angle measured in data. Whilst the absolute measurement of the Cherenkov angle for pure C_4F_{10} was, therefore, not possible, the Sellmeier tuning method allowed an accurate comparison between data and simulation of the Cherenkov angle resolution. Assuming a 90/10 admixture of C_4F_{10}/N_2 in the simulation gave a residual shift of 0.65 mrad in the mean of the simulated distribution compared to data. This was attributed to imperfect knowledge of the actual C_4F_{10} fraction, as well as temperature and atmospheric pressure effects. This residual shift was then corrected for by fine-tuning in the simulated events.

In order to extract the Cherenkov angle resolution, each θ_C distribution is described by a double-Gaussian with common mean. The Cherenkov angle resolution is taken as the width of the core distribution. For the case of N_2, the resolution is measured as $\sigma_\theta = (0.296 \pm 0.003\,(\text{stat.}))$ mrad and agrees well with the value obtained for simulated events $\sigma_\theta = (0.290 \pm 0.003\,(\text{stat.}))$ mrad. The resolution in events recorded with C_4F_{10} is determined as $\sigma_\theta = (0.166 \pm 0.002\,(\text{stat.}))$ mrad which agrees well with the value obtained for simulated events, $\sigma_\theta = (0.174 \pm 0.005\,(\text{stat.}))$ mrad. The additional tails in the data compared to the simulation are due to residual background effects such as electronic noise and reflection of Cherenkov photons off the HPD mechanical structure which are not yet modelled in the full LHCb simulation software.

The contributions to the Cherenkov angle resolution and systematic uncertainties have been evaluated using the LHCb simulation software. A summary of the contributions to the Cherenkov angle resolution is given in Table 5. The contribution from the photon reconstruction is dominated by pixelisation
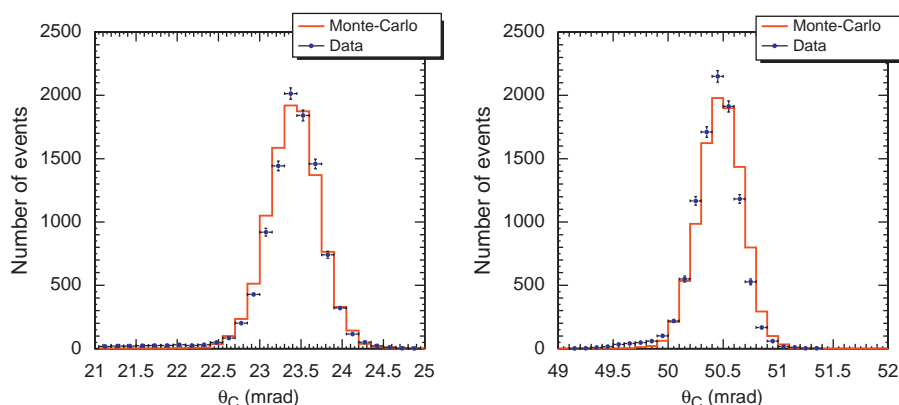
Fig. 8. Per track Cherenkov angle distribution for real (data points) and simulated data (histogram) for a single data run. The left figure shows the Cherenkov angle measured in N_2, the right figure shows the result obtained when using C_4F_{10} as radiator medium.

Table 5
Contributions to the Cherenkov angle resolution.

Effect	Contribution (mrad)	
Photon reconstruction	0.25	(N_2)
	0.13	(C_4F_{10})
Charge sharing	0.03	(N_2)
	0.02	(C_4F_{10})
Chromatic effects	0.12	(N_2)
	0.11	(C_4F_{10})
Beam reconstruction	Negligible	
Added in quadrature	0.28	(N_2)
	0.17	(C_4F_{10})

Table 6
Summary of the systematic uncertainties of the Cherenkov angle resolution.

Effect	Syst. uncertainty (mrad) (N_2)	Syst. uncertainty (mrad) (C_4F_{10})
Charge sharing	0.005	0.002
Mirror alignment	0.004	0.001
Added in quadrature	0.006	0.002

The contributions are evaluated using simulated events.

effects and the point-spread function. The point-spread function is defined as the RMS of the photoelectron distribution at the silicon pixel sensor due to a point source at the cathode, and has been measured in the laboratory. The influence due to the pixelisation effects is mainly due to the compact geometry of the beam-test and HPD pixelisation will not be dominant in the final LHCb RICH detectors. The contribution due to the beam reconstruction is found to be negligible in this analysis due to the long baseline of the beam and the use of dedicated tracking stations as part of the test setup. The systematic uncertainties from the mirror alignment and charge-sharing effect are summarised in Table 6.

5. Conclusions

A set of 48 Hybrid Photon Detectors and readout electronics from the final production of the LHCb RICH detectors has been tested at the SPS facility at CERN. Using a beam matching the 25 ns structure of the LHC, it has been successfully demonstrated that all aspects of the RICH operation meet the stringent requirements of the LHCb experiment. The data have been recorded using the LHCb data-acquisition software and the results obtained using the full LHCb simulation and reconstruction framework. Key elements in the evaluation of the performance of the RICH detectors are the photon yield and the Cherenkov

angle resolution. Both quantities have been measured using N_2 and C_4F_{10} as radiators. The Cherenkov angle resolutions are measured to be $\sigma_\theta = (0.296 \pm 0.003\ \text{(stat.)} \pm 0.006\ \text{(syst.)})\,\text{mrad}$ for N_2 and $\sigma_\theta = (0.166 \pm 0.002\ \text{(stat.)} \pm 0.002\ \text{(syst.)})\,\text{mrad}$ for C_4F_{10}, in line with expectations. Both the measured resolution and the photon yield confirm the results of previous beam-tests [4] and agree with simulation. All components of the RICH detectors are now installed in the LHCb and, based on these results, we expect excellent performance.

References

[1] The LHCb Collaboration, The LHCb Detector at the LHC, JINST 3 S08005 (2008).
[2] LHCb RICH Technical Design Report, CERN/LHCC/2000-037, LHCb TDR 3, September 2000.
[3] M. Moritz, et al., IEEE Trans. Nucl. Sci. NS-51 (3) (2004) 31.
[4] M. Adinolfi, et al., Nucl. Instr. and Meth. A 574 (2007) 39.
[5] M. Alemi, et al., TA2 Collaboration, Nucl. Instr. and Meth. A 449 (2000) 48.
[6] C. Iselin, Solution of Poissons or Laplacés equation in two-dimensional regions, CERN Program Library, long write-up T604, 1984.
[7] T. Seidel, Calculation of photoelectron paths in cylindrical coordinates, CERN EF/IN Internal Report, Program updated by T. Gys, 1990.
[8] M. Adinolfi, et al., Nucl. Instr. and Meth. A 572 (2007) 689.
[9] K. Wyllie, LHCb-RICH Collaboration, Nucl. Instr. and Meth. A 567 (2006) 184.
[10] C. Arnaboldi, T. Bellunato, E. Panzeri, G. Pessina, T. Gys, D. Piedigrossi, IEEE Trans. Nucl. Sci. NS-53 (2006) 1397.
[11] J. Christiansen, A. Marchioro, P. Moreira, T. Toifl, TTCrx: timing, trigger and control receiver ASIC, CERN/EP/MIC, 1999.
[13] Landolt-Börnstein, Eigenschaften der Materie in ihren Aggregatzuständen, 8. Teil Optische Konstanten; P.W. Langhoff, M. Karplus, J. Opt. Soc. Am. 59 (1969) 863.
[14] T.A. Filippas, E. Fokitis, S. Maltezos, K. Patrinos, M. Davenport, Nucl. Instr. and Meth. B 196 (2002) 340.
[15] T. Ypsilantis, J. Seguinot, Nucl. Instr. and Meth. A 343 (1994) 30.
[16] S. Agostinelli, et al., Nucl. Instr. and Meth. A 506 (2003) 250.
[17] W. Baldini, et al., LHCb Collaboration, Overview of LHCb alignment, CERN LHCb 2006-035.
[18] H. Atherton, et al., CERN Yellow Report 80-07, 1980.
[19] N. Kanaya, et al., Performance study of hybrid photon detectors for the LHCb RICH, in: Proceedings of the fifth International Workshop on Ring Imaging Detectors, Nucl. Instr. and Meth. A 553 (1–2) (2005) 41.
[20] R. Forty, LHCb Collaboration, Nucl. Instr. and Meth. A 433 (1999) 257.